Published in final edited form as:
Sci Signal. ; 5(236): . doi:10.1126/scisignal.2002829.

Microtubules Underlie Dysfunction in Duchenne Muscular Dystrophy

Ramzi J. Khairallah[1], **Guoli Shi**[2], **Francesca Sbrana**[3,4], **Benjamin L. Prosser**[1], **Carlos Borroto**[2], **Mark J. Mazaitis**[5], **Eric P. Hoffman**[6,7], **Anup Mahurkar**[5], **Fredrick Sachs**[8], **Yezhou Sun**[5], **Yi-Wen Chen**[6,7], **Roberto Raiteri**[3], **W. Jonathan Lederer**[1], **Susan G. Dorsey**[2,*], and **Christopher W. Ward**[2,*]

[1]Center for Biomedical Engineering and Technology and Department of Physiology, University of Maryland School of Medicine, Baltimore, MD 21201, USA.

[2]University of Maryland School of Nursing, Baltimore, MD 21201, USA.

[3]Department of Biophysical and Electronic Engineering, Università di Genova, Genova 12126, Italy.

[4]Biophysics Institute, National Research Council, Genova 16149, Italy.

[5]Institute for Genome Sciences, University of Maryland School of Medicine, Baltimore, MD 21201, USA.

[6]Research Center for Genetic Medicine, Children's National Medical Center, George Washington University, Washington, DC 20010, USA.

[7]Department of Integrative Systems Biology, George Washington University, Washington, DC 20010, USA.

[8]Center for Single Molecule Studies, University of Buffalo and Tonus Therapeutics, Buffalo, NY 14260, USA.

Abstract

Duchenne muscular dystrophy (DMD) is a fatal X-linked degenerative muscle disease caused by the absence of the microtubule-associated protein dystrophin, which results in a disorganized and denser microtubule cytoskeleton. In addition, mechanotransduction-dependent activation of calcium (Ca^{2+}) and reactive oxygen species (ROS) signaling underpins muscle degeneration in DMD. We show that in muscle from adult mdx mice, a model of DMD, a brief physiologic stretch elicited microtubule-dependent activation of NADPH (reduced-form nicotinamide adenine dinucleotide phosphate) oxidase–dependent production of ROS, termed X-ROS. Further, X-ROS amplified Ca^{2+} influx through stretch-activated channels in mdx muscle. Consistent with the importance of the microtubules to the dysfunction in mdx muscle, muscle cells with dense microtubule structure, such as those from adult mdx mice or from young wild-type mice treated with Taxol, showed increased X-ROS production and Ca^{2+} influx, whereas cells with a less dense

*To whom correspondence should be addressed. ward@son.umaryland.edu (C.W.W.); sdorsey@son.umaryland.edu (S.G.D., regarding the transcriptome analysis). Back.

Author contributions: R.J.K., C.W.W., B.L.P., F.S., R.R., and W.J.L. designed the experiments. R.J.K., C.W.W., G.S., F.S., and R.R. performed the experiments and analyzed the data. S.G.D., C.B., A.M., Y.S., Y.-W.C., E.P.H., C.W.W., and R.J.K. performed transcriptional profiling and analyzed the data. R.J.K. and C.W.W. wrote the paper. B.L.P., M.J.M., and W.J.L. assisted with manuscript preparation. Competing interests: F.S. is the president of Tonus Therapeutics, which holds a patent on GsMTx4. C.W.W. and R.J.K. have applied for a patent for the therapeutic use of X-ROS targets that encompass microtubule-destabilizing drugs and NOX2 inhibitors for the treatment of neuromuscular disease (U.S. Patent Application No. 61/562,527). The other authors declare that they have no competing interests.

microtubule network, such as young mdx or adult mdx muscle treated with colchicine or nocodazole, showed little ROS production or Ca^{2+} influx. In vivo treatments that disrupted the microtubule network or inhibited NADPH oxidase 2 reduced contraction-induced injury in adult mdx mice. Furthermore, transcriptome analysis identified increased expression of X-ROS–related genes in human DMD skeletal muscle. Together, these data show that microtubules are the proximate element responsible for the dysfunction in Ca^{2+} and ROS signaling in DMD and could be effective therapeutic targets for intervention.

Introduction

Duchenne muscular dystrophy (DMD) is a devastating and fatal X-linked degenerative muscle disease that affects about 1 in 3500 male births. Although it is unequivocal that the absence of dystrophin is the molecular cause of DMD (1), the latency of disease presentation and spectrum of disease severity (2, 3) suggests that the absence of dystrophin alone does not explain the downstream muscle weakness and wasting. For example, several genetic factors have been identified that contribute to the onset and pathogenic progression of the disease (2, 3).

In human patients with DMD as well as in the most widely used murine model of DMD (the mdx mouse), mechanical stress–dependent dysregulation of Ca^{2+} and reactive oxygen species (ROS) signaling is a critical factor in the dystrophic process (4–6). In response to membrane stressors (such as isometric and eccentric contraction, acute osmotic challenge, and membrane deformation with suction), mdx myofibers demonstrate an inability to maintain a low myoplasmic concentration of Ca2+ compared with wild-type myofibers, largely because of increased sarcolemmal Ca^{2+} influx through mechanosensitive Ca^{2+} channels (7–11). With the same perturbation, increased ROS production is also evident in mdx fibers leading to increased Ca^{2+} signaling dysfunction through oxidation of Ca^{2+} channels (12, 13).

Membrane stress induces ROS production within the skeletal muscle transverse tubule (14) by activating NADPH (reduced-form nicotinamide adenine dinucleotide phosphate) oxidase 2 (NOX2) (15) through a mechanotransduction-dependent pathway. In conjunction with NOX2-dependent ROS production in mdx muscle, ROS production has also been identified following Ca^{2+} entry into the mitochondria (16, 17). Acting independently or synergistically with Ca^{2+} influx, mechanical stress–induced ROS production has been proposed as a mechanism for the increase in susceptibility to muscle damage in mdx mice (4, 6,18). Despite these advances in understanding the contribution of mechanical stress to muscle dysfunction in DMD, the mechanistic details of the mechanotransduction-dependent activation of Ca^{2+} and ROS pathways are limited.

The microtubule cytoskeleton resists mechanical perturbation in cells and, in doing so, acts as a mechanotransducer (19–22). Dystrophin is a microtubule-associated protein (23), and NOX2 is activated by mechanotransduction (5, 14, 15) through Rac1 as the mechanosensitive element interacting with microtubules (24–26). In the heart, the microtubule network is critical for mechanotransduction-dependent activation of Ca^{2+} (27, 28) and NOX2-dependent ROS (27) signaling during diastolic stretch. Here, we test the hypothesis that the microtubule network plays a role in the enhanced mechano-activation of ROS and Ca^{2+} signaling seen in dystrophic skeletal muscle.

Results

We developed MuST (muscle stretch tool; fig. S1), a technology enabling us to establish a minimal model of stretch-activated mechanotransduction in skeletal muscle that avoids

potential confounders of membrane-damaging force (eccentric injury), exercise, or nonphysiologic stress such as osmotic shock. We used MuST to impose a brief (5 s) and small (~10% sarcomere length) axial stretch on intact flexor digitorum brevis (FDB) muscle fibers. In wild-type myofibers loaded with a fluorescent ROS probe (6–carboxy-2',7'-dichlorodihydrofluorescein diacetate, di-acetoxymethyl ester), axial stretch elicited a small nonsignificant (~7%) increase in ROS production. In contrast, stretch elicited a large (~40%), rapid increase in ROS production in adult mdx myofibers (Fig. 1A and fig. S2).

Cytoskeletal networks propagate mechanical signals throughout muscle cells (29). The absence of the microtubule-associated protein dystrophin results in a disorganized and denser microtubule cytoskeleton (23). In adult mdx muscle, depolymerization of the microtubule cytoskeleton with colchicine (Fig. 1B) or nocodazole (fig. S3) or inhibition of the Rac1 guanosine triphosphatase (fig. S3) ameliorated stretch-induced ROS production, whereas depolymerization of the actin cytoskeleton with latrunculin A (fig. S3) or inhibition of nitric oxide synthase with L-NAME (fig. S3) had no effect.

NOX2 is activated by mechanotransduction (27) and is critical in the pathology of DMD (5). Inhibition of NOX2 with gp91dsTAT (30) (Fig. 1C) or fulvene-5 (31) (fig. S3) verified NOX2 as the source of the stretch-dependent ROS in adult mdx muscle fibers. We thus conclude that in adult mdx muscle, the microtubule network is responsible for the transmission of mechanotransduction signals through NOX2 to generate ROS, a process we have described in the heart and called X-ROS (27).

Dysregulated Ca^{2+} signaling is a hallmark of the dystrophic process, and here we show that a brief stretch significantly increased the rate of cytosolic Ca^{2+} accumulation in adult mdx muscle fibers (~5-fold) when compared with wild-type muscle fibers (~0.2-fold) (Fig. 1D). Consistent with our use of axial stretch as a physiologic perturbation, we did not observe Ca^{2+} sparks in mdx muscle, unlike those reported with osmotic shock (32). The increase in myoplasmic concentration of Ca^{2+} with stretch was independent of sarcoplasmic reticulum release because inhibition of ryanodine receptors did not block Ca^{2+} influx (-0.005 ± 0.046 pre-stretch rate compared with 0.751 ± 0.296 stretch rate). Furthermore, we demonstrated that the stretch-dependent increase in the concentration of Ca^{2+} was due to sarcolemmal Ca^{2+} influx into the myocyte through enhanced activation of stretch-activated Ca^{2+} channels (SACs) because it was ablated by the SAC blocker GsMTx4 (33, 34) (Fig. 1E). Finally, stretch-dependent Ca^{2+} influx was ablated by the microtubule-depolymerizing agent colchicine and the NOX2 inhibitor gp91dsTAT, revealing that X-ROS signaling is responsible for the enhanced mechanotransduction-dependent Ca^{2+} influx in mdx muscle fibers (Fig. 1E).

Western blotting revealed a significant increase in the abundance of NOX2's catalytic (gp91phox), regulatory (p67phox), and microtubule-associated (Rac1) subunits (Fig. 1F). These increases were independent of immune cell infiltration because adult mdx muscle showed lower immune cell counts than did young mdx muscle (fig. S4), which is consistent with other reports (35). Furthermore, the abundance of microtubule subunits (Fig. 2, A and B) and microtubule network density (Fig. 2, C and D, and fig. S5), all essential components of X-ROS, was also increased. A denser microtubule network is more resistant to axial compression of the membrane (19–21, 36). Consistent with these reports, we measured near-membrane mechanical properties with atomic force microscopy (AFM) and showed an increase in near-membrane stiffness in adult mdx muscle compared with wild-type muscle (Fig. 2E).

In DMD, enhanced signaling through mechanotransduction-activated pathways increases susceptibility to muscle damage (5). Furthermore, reports suggest a temporal progression in

the susceptibility to stretch-induced damage of mdx muscle (37, 38). We examined young mdx muscle (~6 to 8 weeks) and showed that the microtubule subunit content (Fig. 2, A and B) as well as membrane stiffness (Fig. 2E) did not differ between young wild-type, young mdx, and adult wild-type muscle fibers when compared with adult mdx. The amount of gp91phox and Rac1 was below the amounts necessary for reliable detection in young mice of each genotype.

In accordance with the temporal progression of X-ROS signaling in mdx muscle, X-ROS, as well as its downstream activation of stretch-dependent Ca^{2+} influx, was significantly increased only in adult mdx muscle fibers, correlating with the increase in X-ROS components in the adult compared with young mdx fibers (Fig. 2, F and G). Young wild-type or young mdx muscle fibers generated X-ROS when the density of the microtubule cytoskeleton was increased with Taxol (Fig. 2H), thus demonstrating the importance of the microtubule network in X-ROS.

In DMD skeletal muscle, mechanical stress activates Ca^{2+} and ROS signaling pathways that contribute to muscle injury (4–6). To test the role of X-ROS in the functional status of mdx muscle, we treated adult mdx mice with either colchicine (to depolymerize microtubules) or apocynin (to inhibit NOX) in vivo to reduce X-ROS signaling and used a contraction protocol to produce mechanical stress. An established isometric contraction protocol in vitro was used to provide a moderate stress challenge that results in force loss only in mdx muscle (39). Treatment with either colchicine or apocynin in vivo significantly decreased the force loss induced by isometric contraction in mdx muscle (Fig. 3, A and B). In the second set of experiments, we used eccentric contractions in vivo (40). As with the isometric contractions, either treatment significantly reduced contraction-induced force loss (Fig. 3, C and D).

Having established X-ROS as a potential therapeutic target in the mdx mouse, we next addressed the potential for X-ROS signaling in human DMD. We conducted a complete transcriptome analysis of clinical diagnostic muscle samples (tables S1 and S2). Because the X-ROS signaling pathway is not a canonical pathway, we constructed a pathway de novo. We found that X-ROS–related transcripts were significantly enriched in human DMD muscle (Fig. 4), including each NOX2 subunit, nine different tubulin isoforms, as well as several SAC candidate genes. In addition, we demonstrated differential enrichment of transcripts for canonical Ca^{2+} pathways. Excitation-contraction coupling–related protein transcripts such as the ryanodine receptor, dihydropyridine receptor subunits, and sarcoplasmic/endoplasmic reticulum calcium adenosine triphosphatase (ATPase) showed decreased abundance, whereas several transient receptor potential (TRP) channels, Orai3, and the sodium-calcium exchanger showed increased abundance. Furthermore, several antioxidant defense proteins, such as catalase, superoxide dismutase, and thioredoxin, showed decreased abundance. All of these changes are consistent with a probable enhancement of X-ROS and sarcolemmal Ca2+ influx in human DMD muscle and support X-ROS as a potential therapeutic target in patients.

Discussion

In mdx myofibers, we used a model of axial stretch to reveal that mechanical stress, transmitted through the microtubule network, activates robust NOX2-dependent ROS production, a pathway called X-ROS (fig. S6). In contrast to adult mdx myofibers, age-matched wild-type or young mdx and wild-type myofibers revealed little or no detectable X-ROS.

The differential magnitude of X-ROS between adult mdx and either adult wild-type or young mdx and wild-type was consistent with both NOX2 subunit content and microtubule

network density or protein abundance being increased in adult mdx myofibers. Indeed, activation of X-ROS in adult mdx was inhibited by either microtubule network destabilization or NOX2 inhibition, suggesting that both played a role in promoting X-ROS generation in adult mdx. However, the proximate role of the microtubule network in X-ROS activation is supported by the ability to induce X-ROS by acutely increasing microtubule network density in young wild-type and mdx myofibers (Fig. 2, C and H). The acute duration of Taxol treatment contradicts any increase in NOX2 subunit or microtubule abundance as a contributor to the increase in X-ROS in mdx. Therefore, we believe that the increase in microtubule network density is solely sufficient for X-ROS.

In response to experimental membrane stressors (for example, eccentric contraction, acute osmotic challenge, or membrane deformation with suction), mdx myofibers cannot maintain a normal low myoplasmic concentration of Ca^{2+}, largely because of increased sarcolemmal Ca^{2+} influx through mechanosensitive Ca^{2+} channels (7–11). Stretch-induced ROS production promotes dysfunctional Ca2+ signaling in mdx muscle due to oxidation of stretch-sensitive sarcolemmal Ca^{2+} channels (12, 13). Because we could inhibit stretch-dependent sarcolemmal Ca^{2+} influx with colchicine, GsMTx4, or gp91dsTAT, we conclude that in adult mdx, the microtubule network is the critical factor that links mechanical stretch to the NOX2-dependent ROS production responsible for sarcolemmal Ca^{2+} channel activation during stretch.

The molecular identity of the stretch-sensitive sarcolemmal Ca^{2+} influx channel remains unclear. A report identified the presence of GsMTx4-sensitive mechanosensitive current density in mdx cells (41) but did not identify the channel involved. Other studies have suggested the involvement of a canonical TRP (TRPC) channel for the increased Ca^{2+} influx in mdx muscle (42), with an increase in mechanosensitive TRPC1 current density due to decreased abundance of Homer protein in mdx muscle (43). We showed that protein transcripts for the ROS-sensitive (44, 45) SAC and SOCE channels (Orai3, TRPC1) were also increased in DMD samples, and Homer 1 transcript was decreased in abundance. Piezo1 and Piezo2 are multipass transmembrane proteins that form mechanically activated cation channels (46) that can be inhibited by GsMTx4 (47), and our transcriptome analysis indicated increased expression of both genes in DMD patients. However, it is still unknown whether these channels are modulated by ROS or whether they might promote X-ROS.

We addressed the direct consequences of increased microtubule density in mdx muscle by near-membrane mechanical measurements with AFM. With AFM probe indentation, we interrogated a very small area of membrane (10–3 μm2) and measured the elastic module within the first 100 nm of the fiber surface (48, 49). This area is composed by external basal membrane, sarcolemma, cytoskeletal network, and some cytoplasm. We found increased transverse stiffness in adult mdx muscle compared with the adult wild-type or young mdx and wild-type muscle. Because the microtubule network acts to resist axial compression (22), this finding is consistent with the notion that the microtubule network decreases the elastic properties within the near-membrane compartment. In fact, our current findings in the adult wild-type and mdx myofibers confirm another report from our group (48).

The molecular basis for the increase in microtubule protein and NOX2 subunit density is unclear. The relative abundance of microtubule and NOX2 protein subunits in the adult mdx compared with the adult wild type is indirectly supported by the increase in mRNA transcript in both mdx mice and human DMD patients. The presence of the transforming growth factor–β (50) and angiotensin (51) signaling pathways in our network is also notable because of reports that both signaling cascades act to increase microtubule protein content and network density (52, 53) and are activated in human DMD muscle. Furthermore, we and

others have shown that inhibition of these pathways is beneficial in both human DMD patients (54) and mdx mice (55).

We directly addressed the potential for X-ROS as a therapeutic target by inhibiting X-ROS components and assaying the protection from contraction-induced injury. The microtubule-depolymerizing agent colchicine is a Food and Drug Administration (FDA)–approved drug used to prevent gout attacks and to treat familial Mediterranean fever (56). Apocynin or its oxidation products inhibit translocation of the cytosolic p47phox and p67phox proteins, causing inactivation of NOX (57). Although apocynin has not been approved by the FDA, it is currently in phase 1 clinical trials for the treatment of chronic obstructive pulmonary disease. In vivo treatment of mdx mice with colchicine or apocynin provided significant protection from both isometric and eccentric injury protocols.

We have presented evidence that microtubule-dependent X-ROS signaling is a unifying mechanism that links the lack of dystrophin to the enhanced mechanotransduction-dependent activation of Ca^{2+} and ROS signaling (fig. S6). We demonstrate that pharmacological targeting of either NOX2 activation or microtubule network stabilization can decrease X-ROS signaling and provide protection from contraction-induced injury. We believe that therapies targeting the microtubule cytoskeleton and NOX2 present novel opportunities for intervention in DMD.

Materials and Methods

All reagents and drugs were purchased from Sigma-Aldrich unless otherwise noted. Taxol was purchased from Invitrogen. Latrunculin A was purchased from Biomol. gp91dsTAT peptide was purchased from Anaspec. Rac1 inhibitor was purchased from Calbiochem. Fulvene-5 was kindly provided by J. Arbiser.

Rodent models

Animal care and procedures were approved and performed in accordance with the standards set by the University of Maryland Institutional Animal Care and Use Committee and by the National Institutes of Health (NIH).

Skeletal muscle isolation

After euthanasia by CO_2 inhalation, FDB muscle was harvested bilaterally and incubated in Dulbecco's modified Eagle's medium with gentamicin (1 μl/ml) and 0.4% collagenase A (Roche Applied Science) as previously described (58, 59). Single intact myofibers were then isolated by gentle trituration. Fibers were imaged or fixed for immunolabeling within an 8-hour period (unless otherwise indicated), thus avoiding morphological changes that can occur in FDB fibers that are cultured for a prolonged period.

Myofiber attachment and stretch

All experiments were performed in a custom rotating glass-bottomed chamber (Four-Hour Day Foundation) equipped with bath perfusion and mounted on a Bio-Rad Radiance fluorescent laser scanning confocal attached to an Olympus IX-70 inverted microscope (Olympus Corp.). Cells were attached with the use of micro-tweezers coated with the biological adhesive MyoTak (IonOptix) and connected to a high-sensitivity force transducer (KG7) equipped with an anti-oscillation filter and a piezoelectric length controller (World Precision Instruments). The force transducer and length controller were mounted on folded motorized micromanipulators (Siskiyou), allowing the placement of tweezers above the cell of interest. The rotating chamber, the tweezer-equipped force transducer and length controller, and the micromanipulators formed the MuST (fig. S1A). Myofibers were

attached at both ends by gently closing the MyoTak-coated tweezers without compressing the cell membrane and then lifting the cell from the bottom of the chamber (fig. S1B). Cell sarcomere length was monitored with a high-speed video sarcomere length camera (fig. S1, C and D; Aurora Scientific), and the length controller was adjusted to produce a stretch equal to 10% of resting sarcomere length. The tension signal from the force transducer and the positional output from the length controller were recorded at 1 kHz with a 600A data acquisition system from Aurora Scientific (fig. S1, E and F).

ROS and calcium influx measurements

ROS was measured as previously described (27) with 6-carboxy-2',7'-dichlorodihydrofluorescein diacetate (DCFH-DA) (Invitrogen) in dimethyl sulfoxide. FDB fibers were suspended in Hepes-buffered Ringer's solution containing 140 mM NaCl, 4.0 mM KCl, 1.0 mM MgSO4, 5.0 mM NaHCO3, 10.0 mM glucose, and 10.0 mM Hepes (pH 7.3) and incubated with Ringer's solution containing DCFH-DA (10 μM) for 30 min at room temperature. DCF-loaded cells were mounted on the MuST and imaged with confocal line-scanning microscopy at 2 ms per line with very low laser intensity to prevent artifactual amplification of the signal due to light oxidation. DCF fluorescence signals were processed as previously described (27). The NOX2-specific inhibitor gp91dsTAT (2 μM) (30), NOX inhibitor fulvene-5 (5 μM) (31), and nitric oxide synthase inhibitor L-NAME (1 mM) were used to verify the source of ROS. Interrogation of cytoskeletal involvement in stretch-dependent ROS or Ca^{2+} influx was done with pharmacological methods. Colchicine (10 μM) or nocodazole (10 μM) was used to depolymerize the microtubule cytoskeleton, and latrunculin A (10 μM) was used to depolymerize the actin cytoskeleton. Taxol (10 μM) was used to increase cytoskeletal network density.

Similar to DCF measurements, FDBs were suspended in Ringer's solution containing 5 μM fluo-4 AM (Invitrogen) for 30 min at room temperature. Fluo-4–loaded cells were mounted on the MuST and imaged by confocal line-scanning microscopy at 2 ms per line. Fluo-4 signal slopes before and after stretch were measured.

When the rate of DCF or Ca^{2+} fluorescence increase was intrinsically low (as in young wild-type myofibers) or inhibited (with gp91dsTAT or GsMTx4), stretch resulted in a decrease in fluorescence rate, a finding consistent with our previous report (27). This result is consistent with both movement artifacts that are inherent with these studies at high spatial and time resolution and the redistribution of mobile dye molecules in the cytosol during stretch. Although we accept this negative deflection in DCF or fluo-4 under low fluorescence conditions as an inherent aspect of this approach, this effect would only contribute to the underestimation of the actual stretch-induced signals we see in this study and would not alter our conclusions.

Western blotting

Western blot analysis was performed as previously described (58). In brief, 20 μg of clarified muscle extract was subjected to SDS–polyacrylamide gel electrophoresis, transferred onto nitrocellulose membranes, and washed/blocked in 5% milk solution in phosphate-buffered saline (PBS) for 1 hour. The membrane was probed overnight with primary antibody at room temperature. The primary antibodies were anti–α-tubulin (DM1A, 1:1000, Sigma-Aldrich), anti–β-tubulin (AA12.1, 1:1000, Developmental Studies Hybridoma Bank), anti–Glu-tubulin (1:1000, Millipore), anti-gp91phox and anti-p67phox (1:1000, BD Transduction Laboratories), anti-Rac1 (1:1000, Millipore), and anti–glyceraldehyde-3-phosphate dehydrogenase (GAPDH) (1:4000, Millipore). Membranes were washed two times for 10 min in 5% milk solution at room temperature and incubated with appropriate secondary antibody (1:10,000) for 1 hour at room temperature, and the

membranes were washed in 0.5% Tween solution in PBS two times for 10 min. Membranes were then exposed to enhanced chemiluminescence with SuperSignal West Pico Chemiluminescent Substrate (Pierce) to develop immunoblots. Blots were imaged and quantified with an imaging system (Syngene, G:Box; GeneTools software). The GAPDH signal served as a loading control.

Immunohistochemistry

Tibialis anterior muscles were flash-frozen (isopentane, ~–40°C) and serially sectioned (16 μm) perpendicular to the fiber axis at the muscle mid-belly. Muscle sections were fixed in paraformaldehyde and stained with antibodies for macrophages (eBioscience, anti-F4/80), $CD4^+$ T cells (BD Biosciences, clone H129.19), and $CD8a^+$ T cells (BD Biosciences, clone 53–6.7). Antibody labeling was visualized with 3,3'-diaminobenzidine peroxidase kit (Vector Labs). The sections were then digitally imaged (Olympus DP70 charge-coupled device camera) on an upright microscope (Olympus BX-50) with a 20× PlanF objective. Immune cells were identified and counted visually by a blind rater. Because of the extremely low occurrence of T cells in these sections, only data on macrophage infiltration (F480 reactivity) were quantified and presented.

Fluorescence labeling and quantification of α-tubulin

Isolated intact FDBs were plated on extracellular matrix gel from Engelbreth-Holm-Swarm murine sarcoma coated imaging dishes (MatTek). After treatment, plated myofibers were fixed with 2% paraformaldehyde, permeabilized with 0.1% Triton X-100 in PBS, blocked in 8% bovine serum albumin in PBS, and then labeled overnight with an antibody to α-tubulin conjugated to Alexa Fluor 488 (antimouse; Invitrogen). Digital images were obtained with a Bio-Rad Radiance fluorescent laser scanning confocal attached to an Olympus IX-70 inverted microscope. Laser intensity was adjusted on a sample-to-sample basis to maximize the amount of microtubules that are visualized. A 35-image Z-stack was taken at 0.5-μm interval, and the most representative nine frames were stacked together with ImageJ (NIH) to form a composite image. Quantification was performed on the binary image representation of the nine-image stack. Background was subtracted uniformly, and the image was transformed into a binary image with ImageJ unbiased binary function. A uniform region of interest was selected and mean intensity was measured.

Atomic force microscopy

Membrane elasticity was measured by nanoindentation. A commercial AFM (5500ILM AFM, Agilent Technologies) equipped with a closed-loop 100-μm scanner was used. The AFM was mounted on top of an inverted optical microscope (model IX70, Olympus), which allows optical access for in situ sample imaging and precise tip positioning. The AFM was equipped with commercial triangular silicon nitride cantilevers with integrated pyramidal tips (Bruker). The cantilever spring constants were evaluated before measurements based on thermal noise, which ensures an accuracy level of 10 to 15%. Two identical cantilevers from the same batch, showing the same calculated spring constant K = 0.011 N/m, were used for all experiments.

Nanoindentation measurements were performed as previously described (49). Briefly, nanoindentation maps were recorded and analyzed with custom software developed in LabVIEW (National Instruments). The AFM tip was positioned on the fiber away from nuclei, and 64 × 64 indentation curves were taken on a 5 × 5 μm2 area in at least three different locations for each fiber. Indentation curves were taken at a constant linear speed (2 μm/s) for both loading and unloading and a maximum indentation depth of 100 nm, which corresponds to an applied load in the order of 0.5 nN. From each map, an average load-

indentation curve and the corresponding elasticity modulus were calculated, approximating the pyramidal shape of the indenter as a cone with a half radius of 19°.

In vitro isometric contraction–induced Injury

After CO_2 asphyxiation and cervical dislocation, single EDL muscles were surgically excised with ligatures at each tendon (5–0 silk suture) and mounted in an in vitro bath between a fixed post and a force transducer (300B-LR, Aurora Scientific) operated in isometric mode. The muscle was maintained in physiological saline solution at 30°C under aeration with 95% O_2/5% CO_2 throughout the experiment. Resting tension, muscle length, and stimulation current were iteratively adjusted for each muscle to obtain optimal twitch force. During a 5-min equilibration, single twitches were elicited every 30 s with electrical pulses (0.5 ms) through platinum electrodes running parallel to the muscle. The injury protocol used to induce a force deficit (39) consisted of 20 maximum isometric contractions (1 s at 100 Hz) separated by 1-min rest periods. The absolute isometric force of each muscle during the contraction protocol was normalized to the maximum isometric force (Po) produced by the muscle during the 20-contraction protocol. The percentage of force decline between the 1st and the 20th contractions was taken as the extent of contraction-induced injury.

In vivo eccentric contraction–induced injury

Eccentric injury of the gastrocnemius muscle was conducted in vivo with a 305B muscle lever system (Aurora Scientific Inc.) as described but with minor modifications. Anesthetized mice (isoflurane) were placed on a thermostatically controlled table; the knee was fixed with a pin and the foot was firmly fixed to a footplate on the motor shaft. Contraction was elicited by percutaneous electrical stimulation of the sciatic nerve. Optimal isometric tetanic torque was determined with increasing current with a minimum of 30 s between each contraction to avoid fatigue. Eccentric contractions at maximal isometric torque (0.2-ms pulse train at 100 Hz) were assayed for the resistance to muscle damage. Eccentric contractions were achieved by translating the footplate 30° backward at a velocity of 40 mm/s after the first 200 ms of the isometric contraction. This protocol consisted of 20 eccentric contractions with 1-min pauses in between. The decrease in the peak isometric force before the eccentric phase was taken as an indication of muscle damage. To test the role of X-ROS in the functional status of mdx muscle, we treated adult mdx mice with either colchicine [1 mg/kg intraperitoneally (ip); 4 hours] or apocynin (3 mg/kg ip; 3 days) in vivo to reduce X-ROS signaling and used a contraction protocol to produce mechanical stress.

Microarray and RNA-seq

The subjects in this study were obtained from referrals for molecular diagnostic services to be performed at the Hoffman laboratory at Children's National Medical Center in Washington, DC. The samples were processed uniformly, and a standard diagnostic set of tests, including biochemical and histological analyses, was performed. These assays included dystrophin immunostaining and immunoblotting and hematoxylin and eosin histological staining, which were performed according to standard methods. RNA or frozen biopsy samples from control subjects (n = 7) with normal muscle pathology and DMD subjects (n = 6) were sequenced (see table S1 for demographic and phenotype information). For microarray studies, we profiled RNA extracted from 6 control subjects and 17 DMD subjects. Total RNA was extracted from frozen muscle biopsies with the standard TRIzol method (Invitrogen). RNA quality and concentration were assayed with a NanoDrop spectrophotometer.

Microarray expression profiling to validate the sequencing data was performed according to the manufacturer's protocols (Affymetrix) (fig. S7). Briefly, total RNA was used to prepare

biotinylated complementary RNA, followed by fragmentation and hybridization to Affymetrix arrays (GeneChip HG-U133Plus2; Affymetrix). The arrays were incubated for about 16 hours, washed, stained, and scanned per the Affymetrix protocol. Differential gene expression through microarray was then performed. We used .cel files generated from Affymetrix profiling process for analysis. Arrays were normalized by the GCRMA (GeneChip Robust Multi-Array) method implemented in GCRMA R package. Differential expression analysis was performed with Linear Models of Microarrays (LIMMA) R package. A linear model was first fitted to expression data for each gene, and the empirical Bayes method was then used to assess differential expression between two conditions. A false discovery rate (FDR) cutoff of less than 0.01 with a twofold change was used to select significant probes.

RNA sequencing was conducted on an Illumina HiSeq System (Illumina Inc.) to obtain 100–base pair paired-end reads. We obtained an average of 148.3 million reads per sample, with an average of 90% of the reads aligning to exonic regions in the genome. These reads were mapped to the GRCh37/hg19 build of the human genome with the short-read aligner TopHat (version 1.2.0). We optimized the parameters segment length, max-multihits, max_cov_juncs, and max_seg_juncs in TopHat to generate contiguous as well as spliced alignments. The alignments were merged to form complete alignments to the genome. These alignments served as the basis of further downstream analyses, including differential gene expression analysis and pathway analysis. Differential gene expression by RNA-seq was then performed. The number of reads mapped on each gene was counted with the HTSeq program (http://www-huber.embl.de/users/anders/HTSeq/) against gene annotation file for GRCh37/hg19 build from Ensembl (http://www.ensembl.org). Read counts were used to measure gene expression. Data normalization and differential expression analysis were performed with the methods implemented in the R package DESeq 1.2 (60). Briefly, DESeq normalizes read counts for sequencing depth and distortion caused by highly differentially expressed genes. A negative binomial model is then used to test the significance of differential expression between two conditions. The criteria used to select significant genes include an FDR cutoff of less than 0.05 with a more than twofold change in gene expression between conditions and a normalized read count of 10 reads per gene in at least one condition.

Gene ontology (GO) analysis on selected significant genes was performed with the R package GOseq (61). Gene length bias existing in RNA-seq was taken into account when the enrichment of the GO category was computed. An FDR cutoff of less than 0.05 was used to select significantly enriched GO categories. We used this information to begin to examine X-ROS signaling components. We interrogated the data for these genes and constructed a pathway with Ariadne Pathway Studio [Ariadne Genomics (Elsevier)] (Fig. 4).

Statistical analysis

Data were analyzed for normality and equal variance. Unless stated otherwise, parametric data were analyzed by one- or two-way analysis of variance (ANOVA) followed by the Holm-Sidak test for multiple comparisons. When assumptions for normality and variance were not met, data were analyzed by one- or two-way ANOVA on ranks with a Dunn's post-test for multiple comparisons. All analyses were conducted with SigmaPlot 11.0 (Systat Software Inc.). Data were presented as means ± SEM, with significance set at $P < 0.05$.

Supplementary Material

Refer to Web version on PubMed Central for supplementary material.

Acknowledgments

We thank S. Martin for reagents and discussion, M. Tedesco for technical assistance with AFM, A. Shetty and T. Creasy for RNA-seq analysis, C. Reggiani for reagents and discussion, J. Arbiser for reagents, L. Michaelson and G. Sinclair (Fourhourday, Baltimore, MD) for technical assistance, and P. Wright for editorial assistance. Funding: This work was supported by NIH grants R01 HL106059, P01 HL67849, R01 HL36974, RC2 NR011968, and U54HD053177. R.J.K. is supported by the Interdisciplinary Training Program in Muscle Biology (T32AR007592). B.L.P. is supported by the Training Program in Cardiovascular Cell Biology (T32 HL072751).

References and Notes

1. Hoffman EP, Brown RH Jr, Kunkel LM. Dystrophin: The protein product of the Duchenne muscular dystrophy locus. Cell. 1987; 51:919–928. [PubMed: 3319190]
2. Pegoraro E, Hoffman EP, Piva L, Gavassini BF, Cagnin S, Ermani M, Bello L, Soraru G, Pacchioni B, Bonifati MD, Lanfranchi G, Angelini C, Kesari A, Lee I, Gordish-Dressman H, Devaney JM, McDonald CM. SPP1 genotype is a determinant of disease severity in Duchenne muscular dystrophy. Neurology. 2011; 76:219–226. [PubMed: 21178099]
3. Nishiyama A, Takeshima Y, Saiki K, Narukage A, Oyazato Y, Yagi M, Matsuo M. Two novel missense mutations in the myostatin gene identified in Japanese patients with Duchenne muscular dystrophy. BMC Med. Genet. 2007; 8:19. [PubMed: 17428346]
4. Allen DG, Gervasio OL, Yeung EW, Whitehead NP. Calcium and the damage pathways in muscular dystrophy. Can. J. Physiol. Pharmacol. 2010; 88:83–91. [PubMed: 20237582]
5. Whitehead NP, Yeung EW, Froehner SC, Allen DG. Skeletal muscle NADPH oxidase is increased and triggers stretch-induced damage in the mdx mouse. PLoS One. 2010; 5:e15354. [PubMed: 21187957]
6. Allen DG, Zhang BT, Whitehead NP. Stretch-induced membrane damage in muscle: Comparison of wild-type and mdx mice. Adv. Exp. Med. Biol. 2010; 682:297–313. [PubMed: 20824533]
7. Marchand E, Constantin B, Vandebrouck C, Raymond G, Cognard C. Calcium homeostasis and cell death in Sol8 dystrophin-deficient cell line in culture. Cell Calcium. 2001; 29:85–96. [PubMed: 11162846]
8. Alderton JM, Steinhardt RA. How calcium influx through calcium leak channels is responsible for the elevated levels of calcium-dependent proteolysis in dystrophic myotubes. Trends Cardiovasc. Med. 2000; 10:268–272. [PubMed: 11282306]
9. Collet C, Csernoch L, Jacquemond V. Intramembrane charge movement and L-type calcium current in skeletal muscle fibers isolated from control and mdx mice. Biophys. J. 2003; 84:251–265. [PubMed: 12524279]
10. Turner PR, Schultz R, Ganguly B, Steinhardt RA. Proteolysis results in altered leak channel kinetics and elevated free calcium in mdx muscle. J. Membr. Biol. 1993; 133:243–251. [PubMed: 8392585]
11. Tutdibi O, Brinkmeier H, Rüdel R, Föhr KJ. Increased calcium entry into dystrophin-deficient muscle fibres of MDX and ADR-MDX mice is reduced by ion channel blockers. J. Physiol. 1999; 515(Pt 3):859–868. [PubMed: 10066910]
12. Isaeva EV, Shirokova N. Metabolic regulation of Ca^{2+} release in permeabilized mammalian skeletal muscle fibres. J. Physiol. 2003; 547:453–462. [PubMed: 12562922]
13. Isaeva EV, Shkryl VM, Shirokova N. Mitochondrial redox state and Ca^{2+} sparks in permeabilized mammalian skeletal muscle. J. Physiol. 2005; 565:855–872. [PubMed: 15845582]
14. Espinosa A, Leiva A, Peña M, Muller M, Debandi A, Hidalgo C, Carrasco MA, Jaimovich E. Myotube depolarization generates reactive oxygen species through NAD(P)H oxidase; ROS-elicited Ca2+ stimulates ERK, CREB, early genes. J. Cell. Physiol. 2006; 209:379–388. [PubMed: 16897752]
15. Hidalgo C, Sánchez G, Barrientos G, Aracena-Parks P. A transverse tubule NADPH oxidase activity stimulates calcium release from isolated triads via ryanodine receptor type 1 S-glutathionylation. J. Biol. Chem. 2006; 281:26473–26482. [PubMed: 16762927]

16. Whitehead NP, Streamer M, Lusambili LI, Sachs F, Allen DG. Streptomycin reduces stretch-induced membrane permeability in muscles from mdx mice. Neuromuscul. Disord. 2006; 16:845–854. [PubMed: 17005404]

17. Whitehead NP, Yeung EW, Allen DG. Muscle damage in mdx (dystrophic) mice: Role of calcium and reactive oxygen species. Clin. Exp. Pharmacol. Physiol. 2006; 33:657–662. [PubMed: 16789936]

18. Allen DG. Skeletal muscle function: Role of ionic changes in fatigue, damage and disease. Clin. Exp. Pharmacol. Physiol. 2004; 31:485–493. [PubMed: 15298539]

19. Ingber DE. Tensegrity and mechanotransduction. J. Bodyw. Mov. Ther. 2008; 12:198–200. [PubMed: 19083675]

20. Stamenovic D, Mijailovich SM, Tolic-Nørrelykke IM, Chen J, Wang N. Cell prestress. II. Contribution of microtubules. Am. J. Physiol. Cell Physiol. 2002; 282:C617–C624. [PubMed: 11832347]

21. Wang N, Naruse K, Stamenovic D, Fredberg JJ, Mijailovich SM, Tolic-Nørrelykke IM, Polte T, Mannix R, Ingber DE. Mechanical behavior in living cells consistent with the tensegrity model. Proc. Natl. Acad. Sci. U.S.A. 2001; 98:7765–7770. [PubMed: 11438729]

22. Wang N, Butler JP, Ingber DE. Mechanotransduction across the cell surface and through the cytoskeleton. Science. 1993; 260:1124–1127. [PubMed: 7684161]

23. Prins KW, Humston JL, Mehta A, Tate V, Ralston E, Ervasti JM. Dystrophin is a microtubule-associated protein. J. Cell Biol. 2009; 186:363–369. [Abstract/Free Full Text]. [PubMed: 19651889]

24. Langevin HM, Bouffard NA, Fox JR, Palmer BM, Wu J, Iatridis JC, Barnes WD, Badger GJ, Howe AK. Fibroblast cytoskeletal remodeling contributes to connective tissue tension. J. Cell. Physiol. 2011; 226:1166–1175. [PubMed: 20945345]

25. Fernandes JJ, Atreya KB, Desai KM, Hall RE, Patel MD, Desai AA, Benham AE, Mable JL, Straessle JL. A dominant negative form of Rac1 affects myogenesis of adult thoracic muscles in Drosophila. Dev. Biol. 2005; 285:11–27. [PubMed: 16125691]

26. Best A, Ahmed S, Kozma R, Lim L. The Ras-related GTPase Rac1 binds tubulin. J. Biol. Chem. 1996; 271:3756–3762. [PubMed: 8631991]

27. Prosser BL, Ward CW, Lederer WJ. X-ROS signaling: Rapid mechano-chemo transduction in heart. Science. 2011; 333:1440–1445. [PubMed: 21903813]

28. Iribe G, Ward CW, Camelliti P, Bollensdorff C, Mason F, Burton RA, Garny A, Morphew MK, Hoenger A, Lederer WJ, Kohl P. Axial stretch of rat single ventricular cardiomyocytes causes an acute and transient increase in Ca2+ spark rate. Circ. Res. 2009; 104:787–795. [PubMed: 19197074]

29. McCain ML, Parker KK. Mechanotransduction: The role of mechanical stress, myocyte shape, and cytoskeletal architecture on cardiac function. Pflugers Arch. 2011; 462:89–104. [PubMed: 21499986]

30. Rey FE, Cifuentes ME, Kiarash A, Quinn MT, Pagano PJ. Novel competitive inhibitor of NAD(P)H oxidase assembly attenuates vascular O2– and systolic blood pressure in mice. Circ. Res. 2001; 89:408–414. [PubMed: 11532901]

31. Bhandarkar SS, Jaconi M, Fried LE, Bonner MY, Lefkove B, Govindarajan B, Perry BN, Parhar R, Mackelfresh J, Sohn A, Stouffs M, Knaus U, Yancopoulos G, Reiss Y, Benest AV, Augustin HG, Arbiser JL. Fulvene-5 potently inhibits NADPH oxidase 4 and blocks the growth of endothelial tumors in mice. J. Clin. Invest. 2009; 119:2359–2365. [PubMed: 19620773]

32. Wang X, Weisleder N, Collet C, Zhou J, Chu Y, Hirata Y, Zhao X, Pan Z, Brotto M, Cheng H, Ma J. Uncontrolled calcium sparks act as a dystrophic signal for mammalian skeletal muscle. Nat. Cell Biol. 2005; 7:525–530. [PubMed: 15834406]

33. Suchyna TM, Tape SE, Koeppe II RE, Andersen OS, Sachs F, Gottlieb PA. Bilayerdependent inhibition of mechanosensitive channels by neuroactive peptide enantiomers. Nature. 2004; 430:235–240. [PubMed: 15241420]

34. Yeung EW, Whitehead NP, Suchyna TM, Gottlieb PA, Sachs F, Allen DG. Effects of stretch-activated channel blockers on [Ca2+]i and muscle damage in the mdx mouse. J. Physiol. 2005; 562:367–380. [PubMed: 15528244]

35. Spencer MJ, Walsh CM, Dorshkind KA, Rodriguez EM, Tidball JG. Myonuclear apoptosis in dystrophic mdx muscle occurs by perforin-mediated cytotoxicity. J. Clin. Invest. 1997; 99:2745–2751. [PubMed: 9169505]
36. Ingber DE. Tensegrity-based mechanosensing from macro to micro. Prog. Biophys. Mol. Biol. 2008; 97:163–179. [PubMed: 18406455]
37. Grange RW, Gainer TG, Marschner KM, Talmadge RJ, Stull JT. Fast-twitch skeletal muscles of dystrophic mouse pups are resistant to injury from acute mechanical stress. Am. J. Physiol. Cell Physiol. 2002; 283:C1090–C1101. [PubMed: 12225973]
38. Wolff AV, Niday AK, Voelker KA, Call JA, Evans NP, Granata KP, Grange RW. Passive mechanical properties of maturing extensor digitorum longus are not affected by lack of dystrophin. Muscle Nerve. 2006; 34:304–312. [PubMed: 16770793]
39. Ng R, Metzger JM, Claflin DR, Faulkner JA. Poloxamer 188 reduces the contraction-induced force decline in lumbrical muscles from mdx mice. Am. J. Physiol. Cell Physiol. 2008; 295:C146–C150. [PubMed: 18495816]
40. Blaauw B, Mammucari C, Toniolo L, Agatea L, Abraham R, Sandri M, Reggiani C, Schiaffino S. Akt activation prevents the force drop induced by eccentric contractions in dystrophin-deficient skeletal muscle. Hum. Mol. Genet. 2008; 17:3686–3696. [PubMed: 18753145]
41. Suchyna TM, Sachs F. Mechanosensitive channel properties and membrane mechanics in mouse dystrophic myotubes. J. Physiol. 2007; 581:369–387. [PubMed: 17255168]
42. Millay DP, Goonasekera SA, Sargent MA, Maillet M, Aronow BJ, Molkentin JD. Calcium influx is sufficient to induce muscular dystrophy through a TRPC-dependent mechanism. Proc. Natl. Acad. Sci. U.S.A. 2009; 106:19023–19028. [PubMed: 19864620]
43. Stiber JA, Zhang ZS, Burch J, Eu JP, Zhang S, Truskey GA, Seth M, Yamaguchi N, Meissner G, Shah R, Worley PF, Williams RS, Rosenberg PB. Mice lacking Homer 1 exhibit a skeletal myopathy characterized by abnormal transient receptor potential channel activity. Mol. Cell. Biol. 2008; 28:2637–2647. [PubMed: 18268005]
44. Bogeski I, Kappl R, Kummerow C, Gulaboski R, Hoth M, Niemeyer BA. Redox regulation of calcium ion channels: Chemical and physiological aspects. Cell Calcium. 2011; 50:407–423. [PubMed: 21930299]
45. Bogeski I, Kummerow C, Al-Ansary D, Schwarz EC, Koehler R, Kozai D, Takahashi N, Peinelt C, Griesemer D, Bozem M, Mori Y, Hoth M, Niemeyer BA. Differential redox regulation of ORAI ion channels: A mechanism to tune cellular calcium signaling. Sci. Signal. 2010; 3:ra24. [PubMed: 20354224]
46. Coste B, Mathur J, Schmidt M, Earley TJ, Ranade S, Petrus MJ, Dubin AE, Patapoutian A. Piezo1 and Piezo2 are essential components of distinct mechanically activated cation channels. Science. 2010; 330:55–60. [PubMed: 20813920]
47. Bae C, Sachs F, Gottlieb PA. The mechanosensitive ion channel Piezo1 is inhibited by the peptide GsMTx4. Biochemistry. 2011; 50:6295–6300. [PubMed: 21696149]
48. Canato M, Dal Maschio M, Sbrana F, Raiteri R, Reggiani C, Vassanelli S, Megighian A. Mechanical and electrophysiological properties of the sarcolemma of muscle fibers in two murine models of muscle dystrophy: Col6a1–/– and mdx. J. Biomed. Biotechnol. 2010; 2010:981945. [PubMed: 20396399]
49. Defranchi E, Bonaccurso E, Tedesco M, Canato M, Pavan E, Raiteri R, Reggiani C. Imaging and elasticity measurements of the sarcolemma of fully differentiated skeletal muscle fibres. Microsc. Res. Tech. 2005; 67:27–35. [PubMed: 16025488]
50. Chen YW, Nagaraju K, Bakay M, McIntyre O, Rawat R, Shi R, Hoffman EP. Early onset of inflammation and later involvement of TGFβ in Duchenne muscular dystrophy. Neurology. 2005; 65:826–834. [PubMed: 16093456]
51. Sun G, Haginoya K, Dai H, Chiba Y, Uematsu M, Hino-Fukuyo N, Onuma A, Iinuma K, Tsuchiya S. Intramuscular renin–angiotensin system is activated in human muscular dystrophy. J. Neurol. Sci. 2009; 280:40–48. [PubMed: 19232644]
52. Stroth U, Meffert S, Gallinat S, Unger T. Angiotensin II and NGF differentially influence microtubule proteins in PC12W cells: Role of the AT2 receptor. Brain Res. Mol. Brain Res. 1998; 53:187–195. [PubMed: 9473667]

53. Hashimoto-Komatsu A, Hirase T, Asaka M, Node K. Angiotensin II induces microtubule reorganization mediated by a deacetylase SIRT2 in endothelial cells. Hypertens. Res. 2011; 34:949–956. [PubMed: 21677656]
54. Ogata H, Ishikawa Y, Ishikawa Y, Minami R. Beneficial effects of β-blockers and angiotensin-converting enzyme inhibitors in Duchenne muscular dystrophy. J. Cardiol. 2009; 53:72–78. [PubMed: 19167641]
55. Cohn RD, van Erp C, Habashi JP, Soleimani AA, Klein EC, Lisi MT, Gamradt M, Ap Rhys CM, Holm TM, Loeys BL, Ramirez F, Judge DP, Ward CW, Dietz HC. Angiotensin II type 1 receptor blockade attenuates TGF-β–induced failure of muscle regeneration in multiple myopathic states. Nat. Med. 2007; 13:204–210. [PubMed: 17237794]
56. Grody WW, Getzug T. Colchicine's other indication—Effect of FDA action. N. Engl. J. Med. 2010; 363:2267–2268. [PubMed: 21121853]
57. Stolk J, Hiltermann TJ, Dijkman JH, Verhoeven AJ. Characteristics of the inhibition of NADPH oxidase activation in neutrophils by apocynin, a methoxy-substituted catechol. Am. J. Respir. Cell Mol. Biol. 1994; 11:95–102. [PubMed: 8018341]
58. Dorsey SG, Lovering RM, Renn CL, Leitch CC, Liu X, Tallon LJ, Sadzewicz LD, Pratap A, Ott S, Sengamalay N, Jones KM, Barrick C, Fulgenzi G, Becker J, Voelker K, Talmadge R, Harvey BK, Wyatt RM, Vernon-Pitts E, Zhang C, Shokat K, Fraser-Liggett C, Balice-Gordon RJ, Tessarollo L, Ward CW. Genetic deletion of trkB.T1 increases neuromuscular function. Am. J. Physiol. Cell Physiol. 2012; 302:C141–C153. [PubMed: 21865582]
59. Ziman AP, Ward CW, Rodney GG, Lederer WJ, Bloch RJ. Quantitative measurement of Ca2+ in the sarcoplasmic reticulum lumen of mammalian skeletal muscle. Biophys J. 2010; 99:2705–2714. [PubMed: 20959112]
60. Anders S, Huber W. Differential expression analysis for sequence count data. Genome Biol. 2010; 11:R106. [PubMed: 20979621]
61. Young MD, Wakefield MJ, Smyth GK, Oshlack A. Gene ontology analysis for RNA-seq: Accounting for selection bias. Genome Biol. 2010; 11:R14. [PubMed: 20132535]
62. Percival JM, Gregorevic P, Odom GL, Banks GB, Chamberlain JS, Froehner SC. rAAV6-microdystrophin rescues aberrant Golgi complex organization in mdx skeletal muscles. Traffic. 2007; 8:1424–1439. [PubMed: 17714427]
63. Baudy AR, Sali A, Jordan S, Kesari A, Johnston HK, Hoffman EP, Nagaraju K. Non-invasive optical imaging of muscle pathology in mdx mice using cathepsin caged near-infrared imaging. Mol. Imaging Biol. 2011; 13:462–470. [PubMed: 20661652]

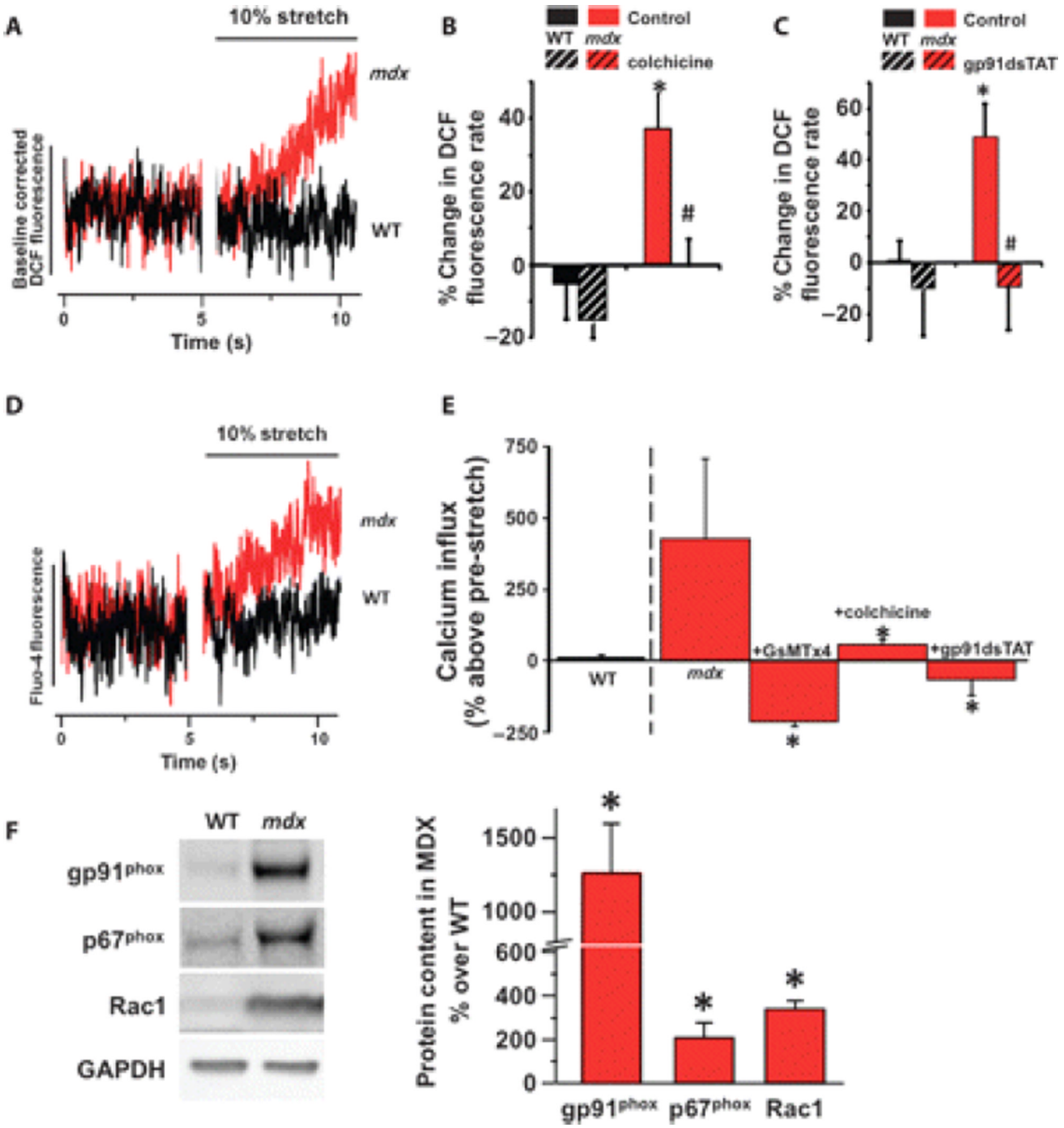

Fig. 1.

X-ROS signaling in dystrophic muscle fibers. (A) Representative averaged data of adult (5 to 6 months) wild-type (WT; n = 5) and mdx (n = 5) single FDB myofibers loaded with DCF and subjected to a 10% stretch. The DCF fluorescence profiles pre- and post-stretch were fit by linear least squares regression. The rates of DCF fluorescence pre- and post-stretch were taken as the rate of ROS production. The DCF fluorescence change was normalized to the pre-stretch to allow comparison of the post-stretch rates. (B) The microtubule polymerization inhibitor colchicine also prevented the increase in X-ROS in mdx. (C) NOX2 inhibition abrogates stretch-induced ROS production in mdx fibers. Fibers from WT (n = 3 animals, 32 fibers) and mdx (n = 3 animals, 23 fibers) were subjected to acute stretch

with a scrambled peptide or with the NOX2 inhibitor gp91dsTAT. Mean values of DCF fluorescence, calculated as percent change over pre-stretch rate, were significantly increased in mdx (*P < 0.05) compared to WT. In mdx fibers, stretch ROS production was inhibited by gp91dsTAT (#P < 0.05). (D) Representative averaged data of 5- to 6-month adult WT and mdx single FDB myofibers loaded with fluo-4. (E) Acute membrane stretch increases sarcolemmal calcium influx in mdx myofibers, as measured by fluo-4 fluorescence rate increase, and is prevented by the SAC inhibitor GsMTx4 (n = 2 animals, 10 fibers), colchicine (n = 3 animals, 12 fibers), and gp91dsTAT (n = 2 animals, 8 fibers) (*P < 0.05 compared to mdx). The increase in the myoplasmic concentration of Ca^{2+} with stretch was independent of sarcoplasmic reticulum release because inhibition of ryanodine receptors did not block Ca^{2+} influx (-0.005 ± 0.046 pre-stretch rate compared to 0.751 ± 0.296 stretch rate; $P < 0.01$ paired t test). (F) Western blot analysis of mdx tibialis anterior muscle displays increased abundance of the NOX2 subunits gp91phox, p67phox, and Rac1 (t test; *P < 0.05 compared to WT).

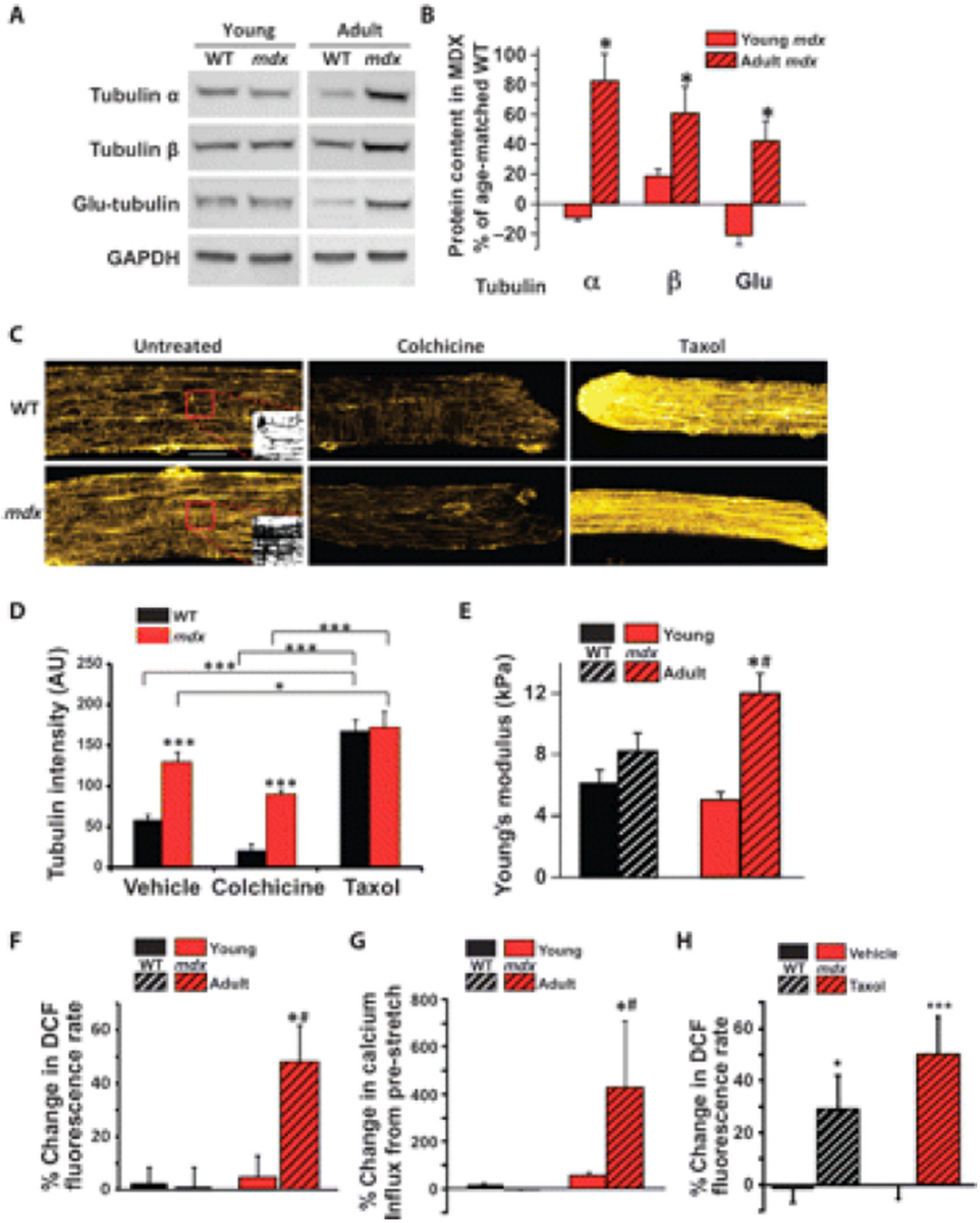

Fig. 2.

Only adult dystrophic muscle displays increased density of the microtubule network, an upstream modulator of X-ROS. (A and B) Adult, but not young, mdx muscle shows increased abundance of the tubulin subunits α and β and increased detyrosination of tubulin (Glu-tubulin) compared to age-matched WT muscle (*P < 0.05 compared to young; n = 6 animals per genotype per age). (C) Immunohistochemistry of α-tubulin reveals that mdx FDB shows a denser microtubule network than WT FDB. Inset panels show binarization of the region of interest (boxed in red). Scale bar, 20 μm. (D) Quantification was performed on binary images of α-tubulin immunohistochemistry (fig. S5; n = 2 animals, 12 fibers per genotype and condition; *P < 0.05, ***P < 0.001). (E) Increased microtubule network

density is accompanied by increased membrane stiffness as measured by AFM (*P < 0.05 compared to young; #P < 0.05 compared to WT). (F and G) Only adult mdx muscle displays (F) X-ROS (n = 2 animals, 14 fibers per genotype; *P < 0.05 compared to young; #P < 0.05 compared to WT) and (G) increased calcium influx (n = 2 animals, 10 fibers per genotype; *P < 0.05 compared to young; #P < 0.05 compared to WT). Data from adult WT and mdx were replotted from Fig. 1, B and D, for comparison. (H) Increasing the microtubule density of young WT and mdx FDBs reveals X-ROS–competent fibers (n = 2 animals, 11 to 14 fibers per genotype; *P < 0.05, ***P < 0.001).

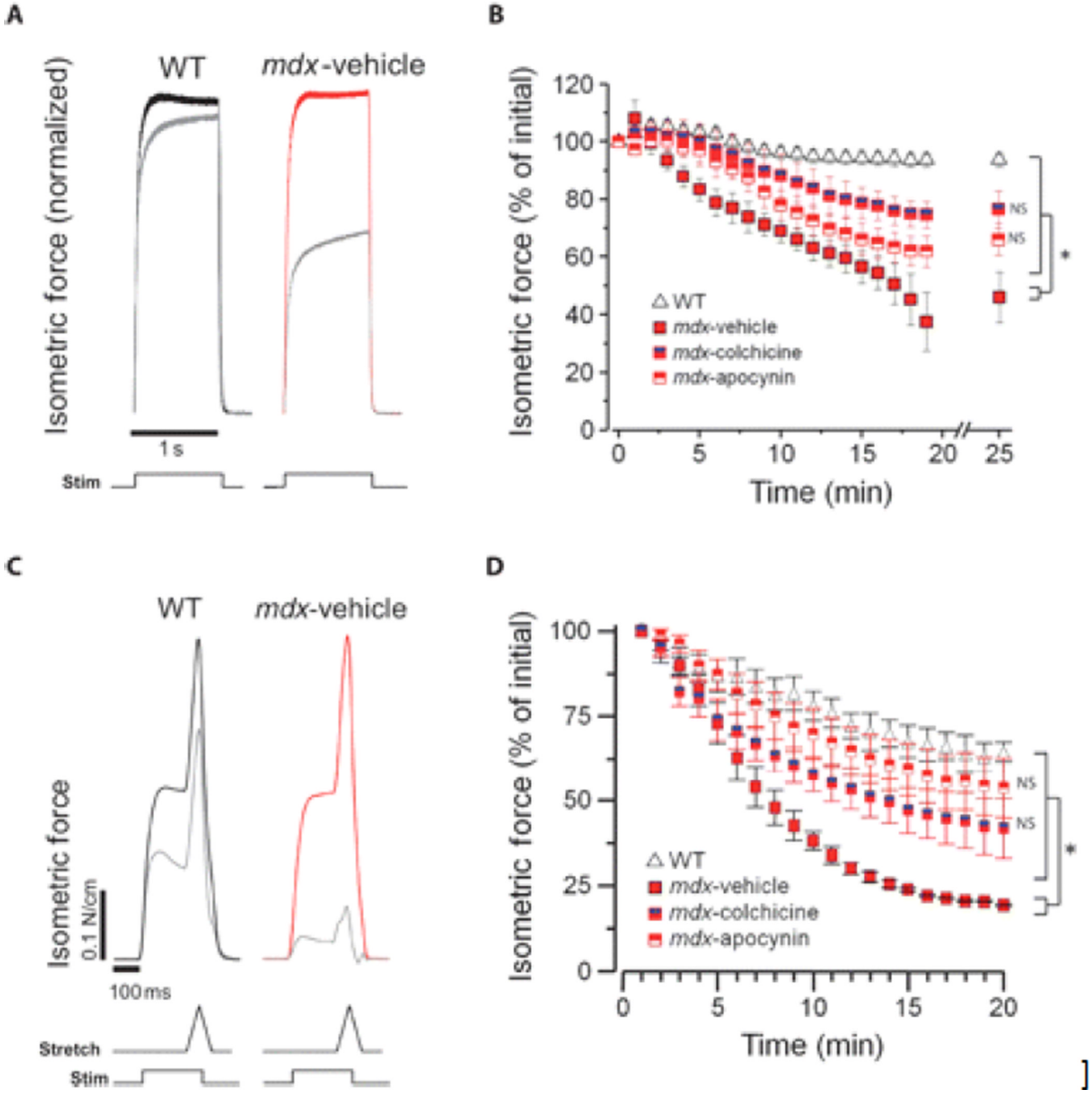

Fig. 3.

In vivo inhibition of X-ROS decreases contraction-induced injury in mdx. (A to D) EDL muscle from mdx mice treated in vivo with vehicle, colchicine, or apocynin was assayed for susceptibility to either in vitro isometric contraction–induced injury (A and B) or in vivo eccentric contraction–induced injury (C and D). Normalized isometric force transients of the initial (t = 0; WT in black, mdx in red) and final (gray) contractions (A and C). WT muscle (n = 4) exhibited little force loss after this protocol, whereas mdx (n = 3) exhibited significant force deficits. Treatment with colchicine (n = 4) or apocynin (n = 4) resulted in a significant protection from force loss (ANOVA: *P < 0.05; NS, not significant compared to WT) (B). WT muscle (n = 3) displayed an ~40% decrease in specific force generation after

20 eccentric contractions, whereas force generation was almost absent in mdx muscle. Treatment with colchicine (n = 4) or apocynin (n = 3) resulted in a significant protection from force loss (ANOVA: *P < 0.05; NS, not significant compared to WT) (D).

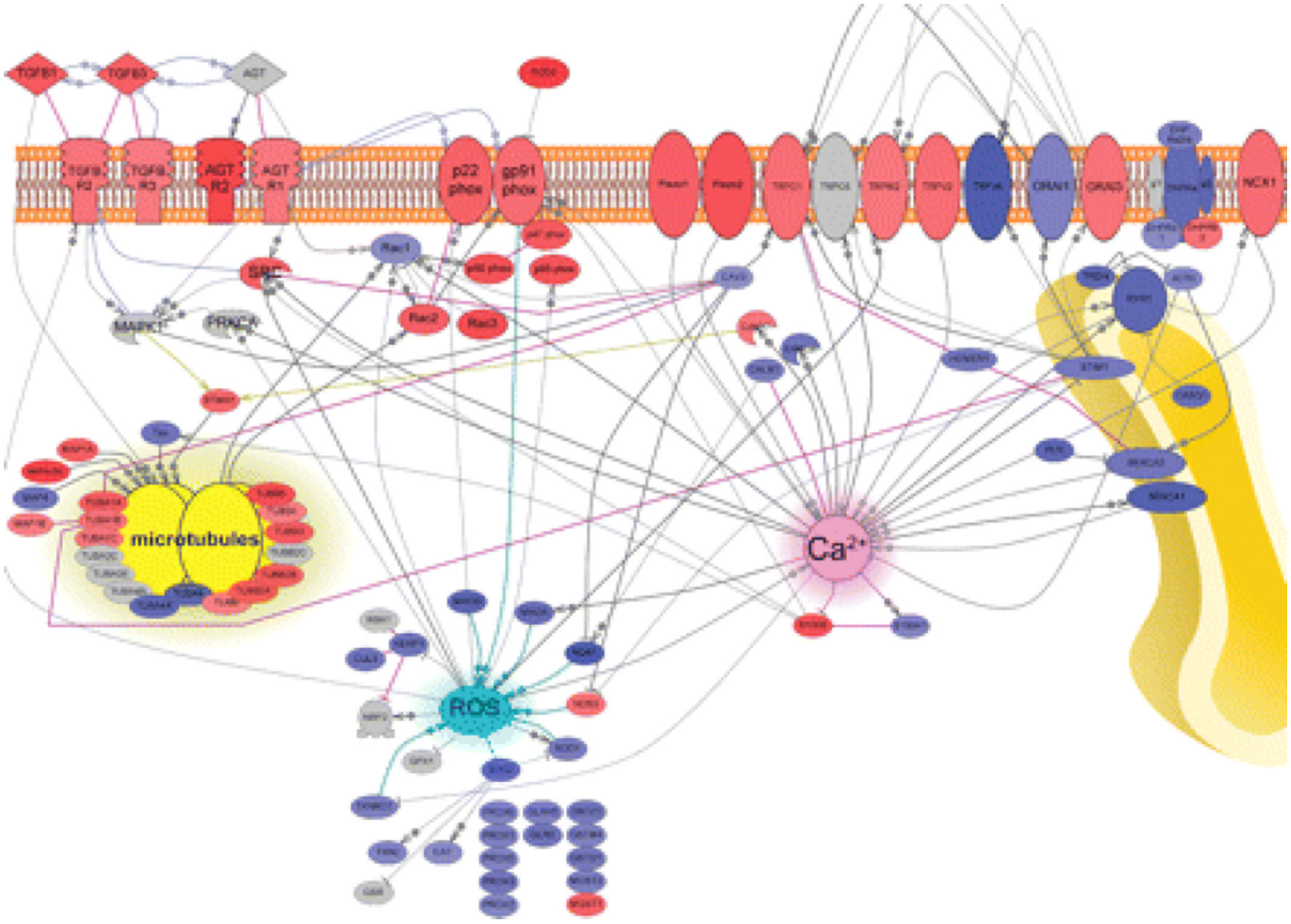

Fig. 4.

Transcriptome analysis of DMD muscle supports the X-ROS signaling mechanism in DMD. Genes in red show significantly increased expression and those in blue show significantly decreased expression in DMD muscle. Arrows represent direct positive regulation. Blunt arrows represent negative regulation. AGT, angiotensin II; AGTR, angiotensin II receptor; CALM, calmodulin; CASQ, calsequestrin; CAT, catalase; CAV3, caveolin 3; CUL3, cullin 3; DHPR, dihydropyridine receptor; GLRX, glutaredoxin; GSR, glutathione S-reductase; GST, glutathione S-transferase; JCTN, junction; MAO, monoamine oxidase; MAP, microtubule-associated protein; NOS, nitric oxide synthase; PLN, phospholamban; PRDX, peroxiredoxin; PRKCA, protein kinase Cα; SERCA, sarcoplasmic/endoplasmic reticulum calcium ATPase; SOD, superoxide dismutase; STMN1, stathmin 1; TGFBR, transforming growth factor–β receptor; TRDN, triadin; TUBA, tubulin α; TUBB, tubulin β; TXN, thioredoxin; TXNRD, thioredoxin reductase. These results from clinical patient samples suggest that the X-ROS signaling pathway operates in human DMD muscle.